



Characterization method for relative Raman enhancement for surface-enhanced Raman spectroscopy using gold nanoparticle dimer array

Sugano, Koji
Ikegami, Kohei
Isono, Yoshitada

(Citation)

Japanese Journal of Applied Physics, 56(6S1):06GK03-06GK03

(Issue Date)

2017-06

(Resource Type)

journal article

(Version)

Accepted Manuscript

(Rights)

©2017 The Japan Society of Applied Physics.

本著作物の利用は、私的利用（著作権法第30条）および引用（著作権法第32条）の範囲内に限られる

(URL)

<https://hdl.handle.net/20.500.14094/90004067>



Characterization method for relative Raman enhancement for surface-enhanced Raman spectroscopy using gold nanoparticle dimer array

Koji Sugano*, Kohei Ikegami, and Yoshitada Isono

*Department of Mechanical Engineering, Graduate School of Engineering, Kobe University,
Kobe 657-8501, Japan*

*E-mail: sugano@mech.kobe-u.ac.jp

In this paper, a characterization method for Raman enhancement for highly sensitive and quantitative surface-enhanced Raman spectroscopy (SERS) is reported. A particle dimer shows a marked electromagnetic enhancement when the particle connection direction is matched to the polarization direction of incident light. In this study, dimers were arrayed by nanotrench-guided self-assembly for a marked total Raman enhancement. By measuring acetonedicarboxylic acid, the fabricated structures were characterized for SERS depending on the polarization angle against the particle connection direction. This indicates that the fabricated structures cause an effective SERS enhancement, which is dominated by the electromagnetic enhancement. Then, we measured 4,4'-bipyridine, which is a pesticide material, for quantitative analysis. In advance, we evaluated the enhancement of the particle structure by the Raman measurement of acetonedicarboxylic acid. Finally, we compared the Raman intensities of acetonedicarboxylic acid and 4,4'-bipyridine. Their intensities showed good correlation. The advantage of this method for previously evaluating the enhancement of the substrate was demonstrated. This developed SERS characterization method is expected to be applied to various quantitative trace analyses of molecules with high sensitivity.

1. Introduction

Surface-enhanced Raman spectroscopy (SERS) is a powerful tool for bio/chemical trace analysis because of its high sensitivity and high molecular identification ability without labeling.¹⁻⁴⁾ A Raman spectrum includes molecular structural information showing several Raman peaks corresponding to a molecular structure. Therefore, it has been expected to be applied to various fields such as medicine, biology, and environment.^{2,5-8)} The Raman scattering light from a small number of molecules is significantly weak. In SERS, however, the Raman scattering light can be enhanced by plasmonic resonance, which occurs on metal nanostructure surfaces.^{2,3)} Therefore, SERS enables us to perform the highly sensitive rapid detection and reliable identification of bio/chemical molecules.

For SERS, various enhancing nanostructures such as those obtained by particle aggregation,^{7,9)} carbon nanotube (CNT) aggregation,¹⁰⁾ and nanoporous fabrication¹¹⁾ have been reported. These nanostructures consist of numerous nanogaps called hotspots. A strategy of these method is to fabricate numerous nanogaps. However, it has been known that Raman enhancement shows a polarization-dependent property of an incident light. Many theoretical studies have supported this polarization dependent Raman enhancement.^{4,12)} Single-molecule SERS detection has been performed using a gold nanoparticle dimer with a molecular bridge between particles when the polarization direction of an incident light is matched to the particle-particle connection direction.^{13,14)} However, the connecting direction cannot be controlled on a substrate for on-substrate SERS measurement.^{12,14)} Moreover, it is necessary to adjust the polarization direction to the connecting direction of particles for each dimer after scanning electron microscopy (SEM) or atomic force microscopy (AFM) observation. Therefore, this method is inefficient for the practical applications of SERS. In addition to the above problems, Raman intensities showed a large variation in the reported SERS experiments. Raman intensity variation has been thought to originate from the distributions of particle arrangement characteristics such as nanogap, particle morphology, the number of hotspots, particle configuration, and particle connecting direction.

To overcome these problems, therefore, we proposed the use of a directionally and regularly arrayed gold nanoparticle dimer as shown in Fig .1. In this structure, two gold nanoparticles configure a particle dimer and dimers are arranged directionally and

regularly on a substrate. Therefore, it is unnecessary to adjust the polarization direction of an incident light for each dimer. A particle dimer is fabricated by drying-based nanotrench-guided self-assembly.¹⁵⁻¹⁹⁾ Particle surfaces are covered by citrate, acetonedicarboxylic acid, acetoacetic acid, and intermediate products after chemical synthesis using a citrate reduction method.²⁰⁻²²⁾ During the drying process in the self-assembly, the adsorbed molecule layer acts as a spacer between particles, forming a nanogap between particles. The thickness of the citrate groups is around 0.5 nm.²³⁾ Therefore, a nanogap of around 1 nm forms between particles. Before the SERS analysis for target molecules in the solution, the adsorbed molecules were removed. Although electron beam (EB) lithography or focused ion beam (FIB) has been used for fabricating orderly nanostructures,¹⁵⁻¹⁹⁾ one cannot fabricate a nanogap of around 1 nm, which shows a marked electromagnetic enhancement.^{24,25)} We confirmed that the proposed structures enable us to perform an ultrasensitive and rapid SERS analysis.^{19,26)}

In our structures, however, the obtained Raman intensities showed large variations as with the previously reported SERS substrates. The distributions of the number of hotspots, particle configuration, and particle connecting direction, mentioned above as reasons for large variations in Raman intensities, should be smaller in our substrate. The Raman intensity variation from our substrate is thought to be due to the distributions of nanogap and particle morphology in the subnanometer scale. The nanogap has a significant effect on Raman enhancement.²⁷⁾ These features are difficult to be controlled.

Therefore, we propose a characterization method for a relative Raman enhancement in this study. A gold nanoparticle chemically synthesized by a citrate reduction method has adsorbed molecules on particle surfaces. We used the adsorbed molecules for preliminary characterization. Although the adsorbed molecules are removed before the SERS analysis for target molecules, Raman intensities from the adsorbed molecules are preliminarily measured for each dimer array. Then, target molecules, 4,4'-bipyridine in this study, are measured after removing the adsorbed molecules. On the basis of the SERS intensities from the adsorbed molecules, we can choose the SERS substrate that shows a higher Raman enhancement. Furthermore, the Raman intensities obtained from target molecules can be compensated using the Raman intensities from the adsorbed molecules. In this study, we evaluated the proposed method by investigating the (1) polarization angle dependence and

(2) Raman intensity relationship between the adsorbed and 4,4'-bipyridine molecules.

2. Experimental and analytical methods

2.1 SERS structure and fabrication process

The directionally and regularly arrayed gold nanoparticle dimers are shown in Fig. 1. In this study, gold nanoparticles with a mean particle diameter of approximately 100 nm were used. The nanoparticles were arranged along the template nanotrenches on a Si substrate using a nanotrench-guided self-assembly method.¹⁶⁻²⁰⁾ The connection direction of the arranged nanoparticles was easily matched to the polarization direction of the incident light without SEM or AFM observation. The intervals of the arranged dimers were 400 and 200 nm in the directions parallel and perpendicular to the coupling direction of the particles, respectively.

The nanotrench-guided self-assembly used in this study is shown in Fig. 2. A colloidal particle solution was injected between a cover glass and a template substrate with an array of nanotrenches. The Si template substrate was etched by inductively coupled plasma reactive ion etching (ICP-RIE) with an EB resist mask pattern. The water surface line moved backward and the particles became concentrated near the meniscus edge during the drying of the aqueous particle dispersion between the substrates. The drag force pressed the particles onto the template substrate to trap the particles on the template nanotrenches when the meniscus passed over the templates. The gold nanoparticles were synthesized by a citrate reduction method. The synthesized particles exhibited negatively charged surfaces because acetonedicarboxylic acid, acetoacetic acid, and citrate molecules uniformly formed and attached to the particle surfaces without vacancy during synthesis.²³⁾ During the removal of the remaining water between the particles, the particles attract each other and form particle-particle contacts, which act as hotspots. A nanogap of around 1 nm forms between particles.

2.2 Characterization method for relative Raman enhancement

Raman measurements were performed using a micro-Raman spectroscopy system equipped with a He-Ne laser of 632.8 nm wavelength. A $\times 50$ objective lens with an NA of 0.5 was used. The laser spot size was approximately 2 μm . For all measurements, mapping Raman measurements were carried out in a $7 \times 7 \mu\text{m}^2$ area with an interval of 1 μm . The center of the mapping area was located at the arrangement area of dimers of $5 \times 5 \mu\text{m}^2$. The integration

time was set to 2 s. The Raman intensities integrated from 1500 to 1700 cm^{-1} were used for characterization because the maximum intensity was observed in that Raman spectra range.

As the first experiment, we investigated the dependence of Raman intensities on the polarization angle of an incident light. In this experiment, the molecules adsorbed on the particle surfaces were used for characterization. After arranging the particles, pure water was placed in a poly(dimethylsiloxane) (PDMS) reservoir, as shown in Fig. 1, and then Raman measurements were carried out. The substrate direction was adjusted through the microscopic observation of the square arrangement area. The polarization angle in the coupling direction was varied from 0 to 90° in 15° increments. The adjustment accuracy was approximately $\pm 1^\circ$. Then, the dependence was compared with the simulation result of the Raman enhancement factor. The Raman enhancement factor $|E|^4$ at the wavelength of an incident light was calculated from the simulated electromagnetic enhancement factor $|E|^2$ at a nanogap.^{12,28-32)} It was simulated by a commercially available finite differential time domain (FDTD) software program. The nanogap between particles was set to 1 nm in this simulation.

Next, we compared the Raman intensities of the adsorbed and 4,4'-bipyridine molecules for the same dimer array. First, we obtained the Raman spectrum of the adsorbed molecules at a polarization angle of 0°. Then, we acquired the Raman spectrum of the 4,4'-bipyridine molecules after removing the adsorbed molecules by UV/O₃ treatment at 80 °C and 40 min. We confirmed from the Raman spectrum that the adsorbed molecules were completely removed. 10^{-3} and 10^{-7} M 4,4'-bipyridine solutions were prepared by dissolving a powder in pure water. The prepared solution was placed in a PDMS reservoir as shown in Fig. 1.

3. Results and discussion

3.1 Fabrication

Figure 3 shows the SEM images of the arrangement of the fabricated gold nanoparticles. We observed that gold nanoparticles were arranged onto the nanotrench template and gold nanoparticle dimers were arrayed directionally and regularly. Although the length of the nanotrench was 260 nm, two particles with a mean diameter of 100 nm were connected by water bridge force during the drying process. All the connection directions of particles were in one direction. In the arranged particles, we found the distributions of particle size, shape,

and the number of hotspots. These distributions are one of the reasons for the observed Raman intensity variations.

3.2 Raman spectroscopy: polarization-dependent property

Figure 4 shows the Raman spectra acquired from the adsorbed molecules on particles surfaces. We observed large broad peaks at Raman shifts from 1000 to 1400 cm^{-1} and from 1500 to 1700 cm^{-1} . These peaks were thought to originate from the adsorbed molecules. These peaks disappeared after the UV/O₃ treatment. The broad peak at around 950 cm^{-1} originated from the Si substrate. The Raman intensity increased with decreasing polarization angle as shown in Fig. 4.

Figure 5 shows the mapping result with the interval of 1 μm . In this result, higher Raman intensities were observed in the $5 \times 5 \mu\text{m}^2$ region, which is the arrangement area. We confirmed that the gold nanoparticle array exhibits a strong enhancement. Figure 6 shows the polarization angle dependences of the normalized experimental Raman intensity and simulated Raman enhancement. These dependences showed good agreement between the experimental and simulation results. The small difference observed at a polarization angle between 15° and 60° is thought to be due to a chemical enhancement effect caused by charge transfer and/or the orientation of molecules adsorbed on particle surfaces. These results indicate that all dimers were arranged in one direction on a substrate and an effective Raman enhancement was possible. Furthermore, Raman intensities were dominated by the electromagnetic enhancement. Therefore, the proposed method using the adsorbed molecules was suitable for the characterization of relative Raman enhancement.

3.3 Raman spectroscopy: 4,4'-bipyridine detection

Figures 7 and 8 show the typical Raman spectra obtained from the adsorbed molecules and 4,4'-bipyridine solution, respectively. The letters in Figs. 7 and 8 indicate the sample numbers. Lines A–C and D–F in Fig. 8 show the Raman spectra obtained from 10^{-3} and 10^{-7} M solutions, respectively, using different substrates. In Fig. 8, several Raman peaks, which originate from 4,4'-bipyridine,³³⁾ are shown as dotted lines. In both cases in Figs. 7 and 8, Raman intensities exhibit large variations.

Figure 9 shows the relationship between the Raman intensities of the adsorbed and 4,4'-bipyridine molecules at 10^{-3} and 10^{-7} M. The letters in Fig. 9 indicate the sample numbers shown in Figs. 7 and 8. They show a linear correlation between the Raman intensities. We

confirmed that the Raman intensities are affected by the SERS structure. The dotted lines indicate the linearly fitted lines. The slopes were 0.123 and 0.062 for 10^{-3} and 10^{-7} M, respectively.

Then, we proposed a compensation method for reducing Raman intensity variations from 4,4'-bipyridine using the obtained correlation slope s . The compensated intensity of 4,4'-bipyridine I_i^P was calculated from $I_i^P = I_i^A + (2000 - I_i^A) \times s$. Here, I_i^A and I_i^P indicate the Raman intensities from the adsorbed and target molecules, respectively. 2000 indicates the standard intensity of the adsorbed molecules, which was determined to be comparable to the average of the adsorbed molecules in this study. This means that the Raman intensity of 4,4'-bipyridine calculated using the obtained slope of the fitting line when the preliminary Raman intensity of the adsorbed molecules is 2000 counts. Figure 10 shows the set of Raman intensities of 4,4'-bipyridine depending on its concentration before and after the compensation shown in Fig. 9. Table I shows a summary of the average, standard deviation, and coefficient value (CV) of Raman intensities. The average intensity at 10^{-3} M was only 1.7 times higher than that of 10^{-7} M. We considered that this is due to the fact that the number of molecules generating the Raman scattering light is not proportional to the molecular concentration owing to the limited number of hotspots and area. The CV values of 4,4'-bipyridine after compensation at 10^{-3} and 10^{-7} M were 10.9 and 11.4%, respectively. The CV was significantly reduced by compensation. The proposed characterization method enables us to choose a highly enhancing SERS substrate and reduce the variation in Raman intensity.

4. Conclusions

In this study, we proposed a characterization method for reducing the variation in Raman intensity for a directionally arrayed gold nanoparticle dimer. The SERS structure was fabricated by nanotrench-guided self-assembly. All particles were connected in one direction.

We confirmed from the polarization dependence that Raman intensities are dominated by the electromagnetic enhancement and that the proposed method using the adsorbed molecules is suitable for the characterization of relative Raman enhancement. These results show a linear correlation between the Raman intensities. We confirmed that the Raman intensities are mainly affected by the SERS structure. The proposed characterization method

enables us to choose a highly enhancing SERS substrate. The CV values of 4,4'-bipyridine after compensation at 10^{-3} and 10^{-7} M were 10.9 and 11.4%, respectively, and CV was significantly reduced by compensation.

Acknowledgments

The Raman spectroscopy experiments were performed at the Kyoto Integrated Science and Technology Bio-Analysis Center (KIST-BIC), sponsored by the Japan Science and Technology Agency (JST). Part of this study was supported by the Kyoto University Nano Technology Hub in the “Nanotechnology Platform Project”, sponsored by the Ministry of Education, Culture, Sports, Science, and Technology, Japan (MEXT). This work was supported by the Japan Society for the Promotion of Science (JSPS) KAKENHI Grant Number 24510138, Grant-in-Aid for Scientific Research (C).

References

- 1) K. Kneipp, H. Kneipp, I. Itzkan, R. R. Dasari, and M. S. Feld, *Chem. Rev.* **99**, 2957 (1999).
- 2) D. Cialla, A. März, R. Böhme, F. Theil, K. Weber, M. Schmitt, and J. Popp, *Anal. Bioanal. Chem.* **403**, 27 (2012).
- 3) S-C. Luo, K. Sivashanmugan, J-D. Liao, C-K. Yao, and H-C. Peng, *Biosens. Bioelectron.* **61**, 232 (2014).
- 4) H. Xu, J. Aizpurua, M. Käll, and P. Apell, *Phys. Rev. E* **62**, 4318 (2000).
- 5) K. Kneipp, H. Kneipp, I. Itzkan, R. R. Dasari, and M. S. Feld, *Curr. Sci.* **77**, 915 (1999).
- 6) C. Otto, T. J. J. van den Tweel, F. F. M. de Mul, and J. Greve, *J. Raman Spectrosc.* **17**, 289 (1986).
- 7) P. C. Pinheiro, S. Fateixa, H. I. S. Nogueira, and T. Trindade, *J. Raman Spectrosc.* **46**, 47 (2015).
- 8) S. E. J. Bell and N. M. S. Sirimuthu, *J. Am. Chem. Soc.* **128**, 15580 (2006).
- 9) R. G. Freeman, K. C. Grabar, K. J. Allison, R. M. Bright, J. A. Davis, A. P. Guthrie, M. B. Hommer, M. A. Jackson, P. C. Smith, D. G. Walter, and M. J. Natan, *Science* **267**, 1629 (1995).
- 10) A. O. Altun, S. K. Youn, N. Yazdani, T. Bond, and H. G. Park, *Adv. Mater.* **25**, 4431 (2013).
- 11) H. Liu, L. Zhang, X. Lang, Y. Yamaguchi, H. Iwasaki, Y. Inouye, Q. Xue, and M. Chen, *Sci. Rep.* **1**, 112 (2011).
- 12) K. Yoshida, T. Itoh, H. Tamaru, V. Biju, M. Ishikawa, and Y. Ozaki, *Phys. Rev. B* **81**, 115406 (2010).
- 13) K. Kneipp, H. Kneipp, V. B. Kartha, R. Manoharan, G. Deinum, I. Itzkan, R. R. Dasari, and M. S. Feld, *Phys. Rev. E* **57**, R6281 (1998).
- 14) S. Nie, and S. Emory, *Science* **275**, 1102 (1997).
- 15) K. Sugano, T. Ozaki, T. Tsuchiya, and O. Tabata, *Sens. Mater.* **23**, 263 (2011).
- 16) T. Ozaki, K. Sugano, T. Tsuchiya, and O. Tabata, *J. Microelectromech. Syst.* **16**, 746 (2007).
- 17) K. Sugano, K. Suekuni, T. Takeshita, K. Aiba, and Y. Isono, *Jpn. J. Appl. Phys.* **54**, 06FL03 (2015).
- 18) T. Takeshita, K. Suekuni, K. Aiba, K. Sugano, and Y. Isono, *Electron. Commun. Jpn.* **100**, 33 (2017).
- 19) K. Sugano, D. Matsui, T. Tsuchiya, and O. Tabata, *Proc. Int. Conf. Micro Electro*

- 255 Mechanical Systems, 2015, p. 608.
- 256 20) S. Kumar, K. S. Gandhi, and R. Kumar, Ind. Eng. Chem. Res **46**, 3128 (2007).
- 257 21) C. H. Munro, W. E. Smith, M. Garner, J. Clarkson, and P. C. White, Langmuir **11**, 3712
258 (1995).
- 259 22) K. Sugano, Y. Uchida, O. Ichihashi, H. Yamada, T. Tsuchiya, and O. Tabata, Microfluid.
260 Nanofluid. **9**, 1165 (2010).
- 261 23) M. Giersig and P. Mulvaney, Langmuir **9**, 3408 (1993).
- 262 24) A. Dhawan, S. J. Norton, M. D. Gerhold, and T. Vo-Dinh, Opt. Express **17**, 9688 (2009).
- 263 25) D. P. Fromm, A. Sundaramurthy, P. J. Schuck, G. Kino, and W. E. Moerner, Nano Lett. **4**,
264 957 (2004).
- 265 26) K. Aiba, K. Ikegami, S. Yamazaki, K. Sugano, and Y. Isono, Denki Gakkai Ronbunshi E
266 **136**, 256 (2016) [in Japanese].
- 267 27) L. Tang, H. Xu, and M. Käll, MRS Bull. **39**, 163 (2014).
- 268 28) D. Radziuk, and H. Moehwald, Phys. Chem. Chem. Phys. **17**, 21072 (2015).
- 269 29) L. A. Lane, X. Qian, S. Nie, Chem. Rev. **115**, 10489 (2015).
- 270 30) Y. S. Yamamoto, M. Ishikawa, Y. Ozaki, T. Itoh, Front. Phys. **9**, 31 (2013).
- 271 31) E. C. Le Ru, P. G. Etchegoin, MRS Bull. **38**, 631 (2013).
- 272 32) H. Perry, A. Gopinath, D. L. Kaplan, L. Dal Negro, F. G. Omenetto, Adv. Mater. **20**, 3070
273 (2008).
- 274 33) M. Suzuki, Y. Niidome, S. Yamada, Thin Solid Films **496**, 740 (2006).
- 275
- 276

Figure Captions

Fig. 1. (Color online) Schematics of proposed and developed gold nanoparticle dimer arrays for SERS, which are fabricated by the nanotrench-guided self-assembly. After particle arrangement the adsorbed molecules cover the particle surfaces. The adsorbed molecules were removed before a Raman measurement for target molecules.

Fig. 2. (Color online) Experimental method for nanoparticle dimer arrangement by nanotrench-guided self-assembly.

Fig. 3. SEM images of gold nanoparticle dimer array: (a) $5 \times 5 \mu\text{m}^2$ region, and (b) enlarged view.

Fig. 4. (Color online) Raman spectra of adsorbed molecules depending on the polarization angle.

Fig. 5. (Color online) Mapping result of adsorbed molecules. The values in the figure show an integral value between 1500 and 1700 cm^{-1} .

Fig. 6. (Color online) Polarization angle dependences of the Raman intensity (experimental: adsorbed molecules) and Raman enhancement (analytical).

Fig. 7. (Color online) Raman spectra of acetone dicarboxylic acid used in the evaluation of the substrate enhancement. The letters indicate the sample numbers.

Fig. 8. (Color online) Raman spectra of 4,4'-bipyridine at 10^{-3} M (A, B, C) and 10^{-7} M (D, E, F). Red dotted lines indicate 4,4'-bipyridine-derived Raman peaks. The letters indicate the sample numbers.

Fig. 9. (Color online) Relationship between Raman intensities of adsorbed molecules and 4,4'-bipyridine at concentrations of 10^{-3} and 10^{-7} M. The letters indicate the sample numbers shown in Figs. 7 and 8.

Fig. 10. (Color online) Raman intensity variations of adsorbed and 4,4'-bipyridine molecules after and before compensation at concentrations of 10^{-3} and 10^{-7} M.

Table I. Average, standard deviation, and CV of Raman intensities of adsorbed and 4,4'-bipyridine molecules after and before compensation at concentrations of (a) 10^{-3} and (b) 10^{-7} M.

(a)				(b)			
	Adsorbed molecule	4,4'-bipyridine	After compensation		Adsorbed molecule	4,4'-bipyridine	After compensation
Average	2185.3	302.2	279.3	Average	1097.2	108.8	165.0
Standard deviation	652.2	86.0	30.5	Standard deviation	731.1	49.3	18.8
CV [%]	29.8	28.5	10.9	CV [%]	66.6	45.3	11.4

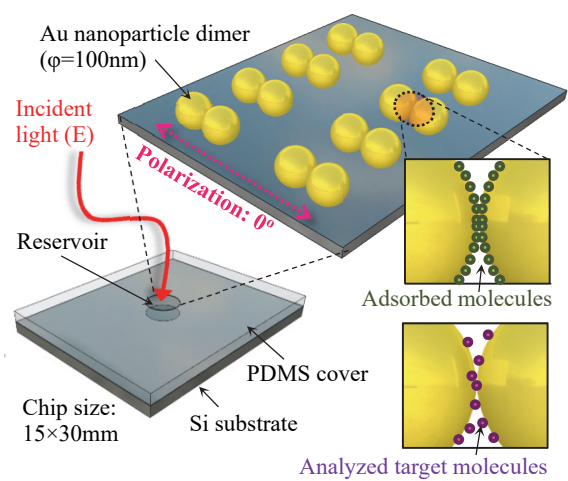


Fig.1. (Color online)

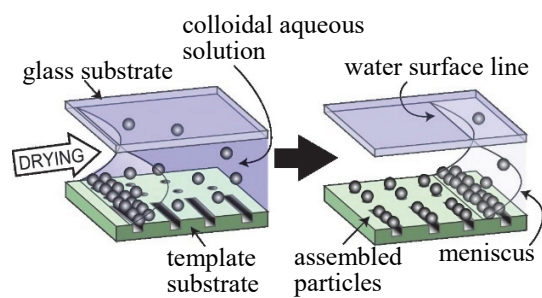


Fig.2. (Color online)

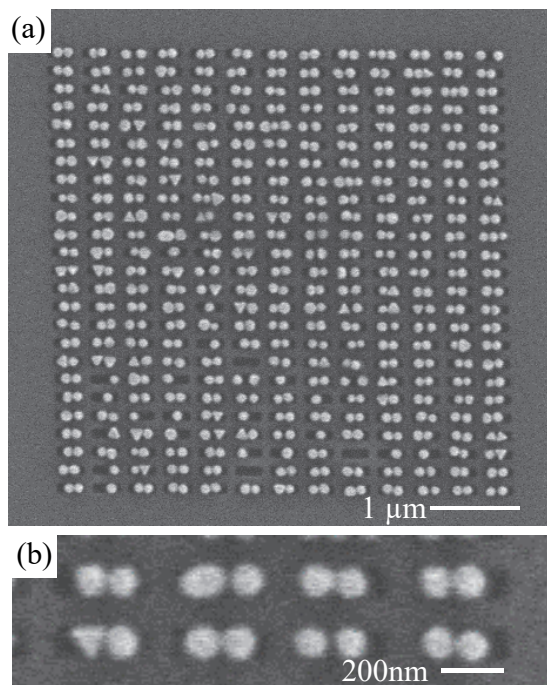


Fig.3.

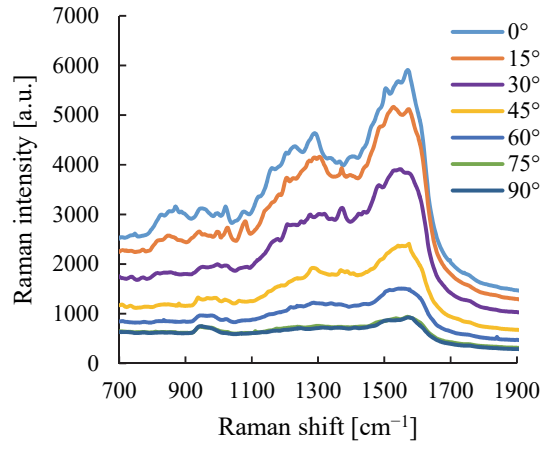


Fig.4. (Color online)

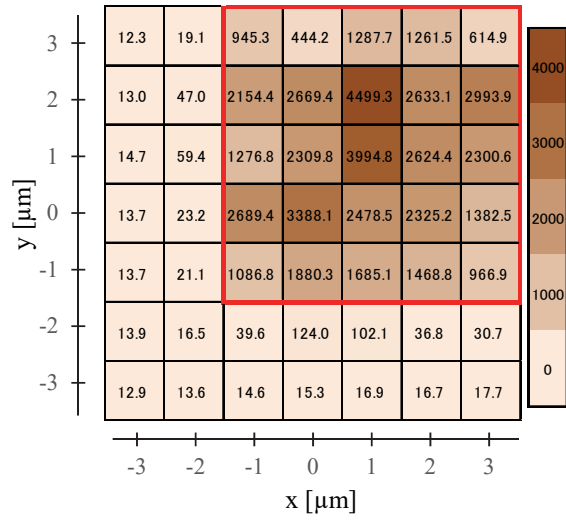


Fig.5. (Color online)

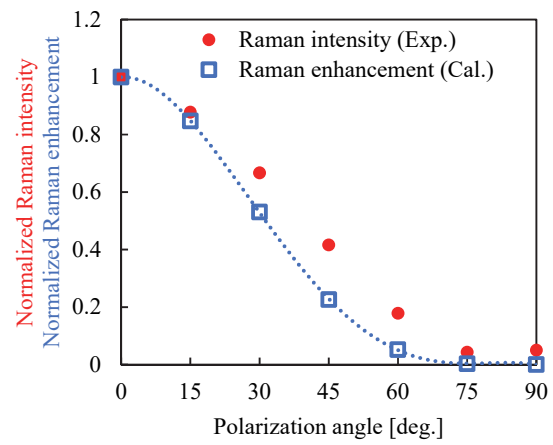


Fig.6. (Color online)

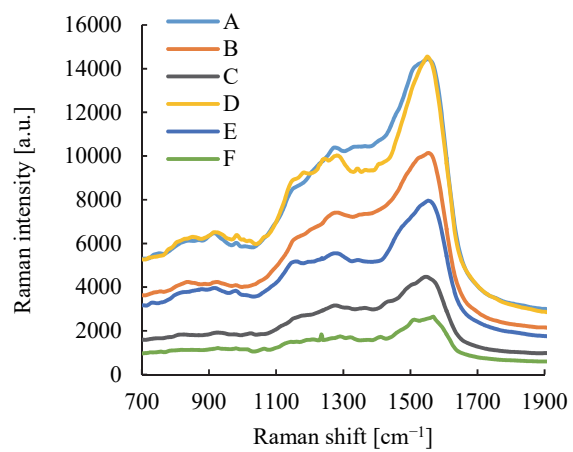


Fig.7. (Color online)

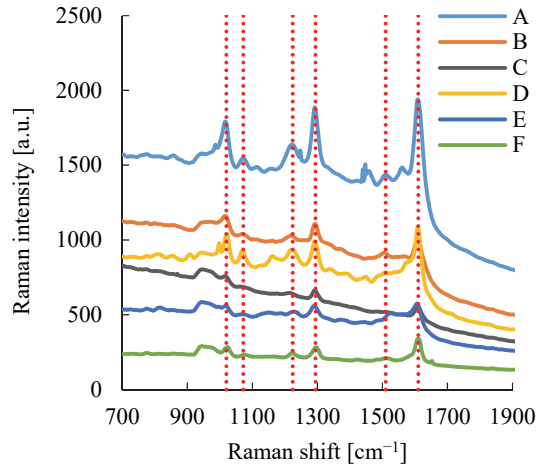


Fig.8. (Color online)

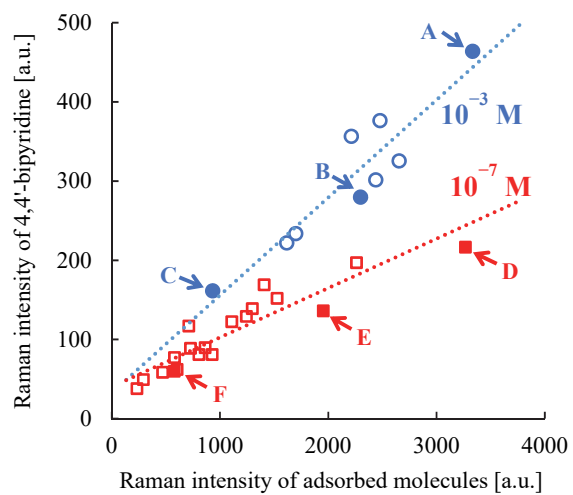


Fig.9. (Color online)

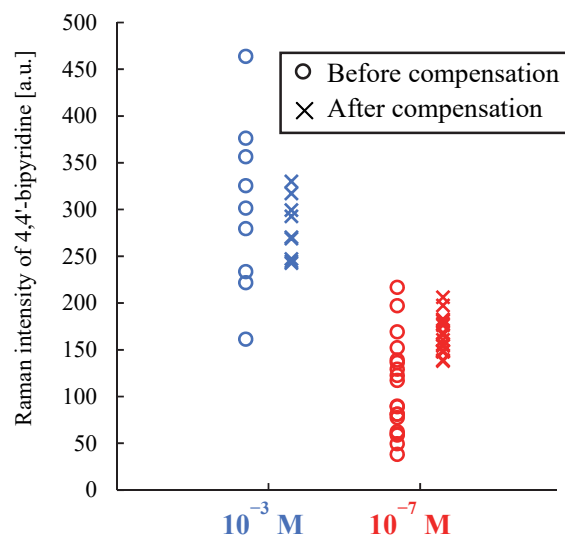


Fig.10. (Color online)